Editors' Suggestion

Rationalizing Euclidean Assemblies of Hard Polyhedra from Tessellations in Curved Space

Philipp W. A. Schönhöfer,[1] Kai Sun,[2] Xiaoming Mao,[2] and Sharon C. Glotzer[1,2,3,*]
[1]Department of Chemical Engineering, University of Michigan, Ann Arbor, Michigan 48109, USA
[2]Department of Physics, University of Michigan, Ann Arbor, Michigan 48109, USA
[3]Biointerfaces Institute, University of Michigan, Ann Arbor, Michigan 48109, USA

(Received 11 May 2023; accepted 20 October 2023; published 21 December 2023)

Entropic self-assembly is governed by the shape of the constituent particles, yet *a priori* prediction of crystal structures from particle shape alone is nontrivial for anything but the simplest of space-filling shapes. At the same time, most polyhedra are not space filling due to geometric constraints, but these constraints can be relaxed or even eliminated by sufficiently curving space. We show using Monte Carlo simulations that the majority of hard Platonic solids self-assemble entropically into space-filling crystals when constrained to the surface volume of a 3-sphere. As we gradually decrease curvature to "flatten" space and compare the local morphologies of crystals assembling in curved and flat space, we show that the Euclidean assemblies can be categorized as either remnants of tessellations in curved space (tetrahedra and dodecahedra) or nontessellation-based assemblies caused by large-scale geometric frustration (octahedra and icosahedra).

DOI: 10.1103/PhysRevLett.131.258201

Introduction.—Particle shape has become an important design parameter in material science [1–3], colloidal self-assembly [4–6], and granular matter [7–9]. One example of the importance of shape is systems of hard particles, which, due solely to entropy maximization, can self-assemble into a zoo of different colloidal crystals simply by changing, even subtly, particle shape [10]. Although methods exist to inversely design particle shapes likely to self-assemble into targeted crystalline structures [11–14], it is nontrivial to predict those structures from particle shape, other than through molecular simulation. This challenge becomes apparent even for the simplest polyhedra, the Platonic solids. Particle shape directly determines both their *assemblies* [10,15]—in which entropy is maximized—and *packings* [10]—in which density is maximized. However, assemblies and packings are the same only for some Platonic solids and polyhedra in general [16]. Cubes are one example where the self-assembled simple cubic (sc) crystal structure and densest packing (a space-filling sc crystal) coincide [17]. Hard octahedra and icosahedra do not fill 3D space, but they, too, maximize entropy in crystals that coincide with their densest packing structures: a rhombohedral and face-centered cubic (fcc) structure, respectively [10,18]. However, hard dodecahedra self-assemble into a 20-particle unit cell β-manganese rotator crystal [10] with two distinct local particle environments instead of its densest packing structure, fcc [18]. Likewise, hard tetrahedra famously form quasicrystals [19,20] with a myriad of different particle environments instead of the putative densest packing structure with a unit cell composed of four tetrahedra arranged in a double-dimer structure [19,21]. Evidently, densest packings, at least in Euclidean space, cannot serve as indicators to predict self-assembly [22,23]. But what of curved space?

Polyhedra fail to self-assemble their densest packing structures when they fail to resolve global geometric constraints that prevent the polyhedra from maximizing entropy locally as well as globally [24]. For example, entropy is maximized for cubes when cube faces are aligned, a motif consistent with the sc densest packing, and thus no geometric constraints arise during assembly. Inspired by studies of Frank-Kasper phases [25–28], glasses [29–35], tetrahelix sheets [36], and liquid crystal blue phases [37–40], we investigate in this Letter if and how hard particle assemblies are related to space-filling tessellations of curved space. We hypothesize that if we can find a suitable space with curvature K that permits a shape to tessellate, then the shape will self-assemble into a crystal based on the tessellation in that space because the tessellating arrangement will maximize entropy. By subsequently flattening the space and monitoring the defects that arise in the process, we posit that we will gain predictive information on the likely structure of the 3D Euclidean assembly.

We first tested our hypothesis by determining if, in positively curved space, any of the five Platonic solids self-assemble entropy maximizing, tessellating 4-polytopes with no global geometric frustration. We performed hard particle Monte Carlo (HPMC) simulations [see Supplemental Material (SM) [41]] and show that tetrahedra, dodecahedra, and octahedra self-assemble into their corresponding 4-polytopes, each in a differently curved space. We then simultaneously increased the 3-sphere

radius $R = K^{-0.5}$ while keeping the packing fraction constant, thereby flattening the curved spaces. This technique geometrically frustrates the assemblies and has shown to increase the kinetic fragility of glass formers [47]. By comparing the local environments of particles assembled in curved and in flat space, we show that the geometric incommensurability, that prevents particles to form entropically favorable tessellations, manifests itself in two different ways as we gradually flatten space. Interestingly, the Euclidean assemblies of tetrahedra and of dodecahedra still exhibit signs of their 3-sphere tessellations. For crystal structures with multiple local environments the geometric frustration suffered by the tessellating assembly as curved space is flattened is resolved by the appearance of defects, leading to an assembly with free volume nonuniformly distributed through the structure. In contrast, we find that the assemblies of octahedra and of icosahedra have a large curvature mismatch between the curved spaces they tessellate and Euclidean space, and thus their 3D assemblies are not related to defect-ridden tessellations from curved space. Instead, shapes which form crystals with unique local environments resolve the geometric frustration in Euclidean space by maximizing entropy uniformly among all the particles, resulting in colloidal crystals of considerably less complexity than those assembled by shapes of type 1.

Self-assembly of 4-polytopes.—The family of regular 4-polytopes can be identified as tessellations of the 3D positively curved volume of a 3-sphere. We performed HPMC simulations of the self-assembly of $N = 600$ tetrahedra, $N = 120$ octahedra, and $N = 24$ dodecahedra with circumsphere diameter σ confined to the 3-sphere into 4-polytopes corresponding to the 600-cell consisting of 600 tetrahedral cells, the 120-cell with 120 dodecahedral cells, and the 24-cell with 24 octahedral cells, respectively. There exist even more tessellations of the three Platonic solids in both hyperbolic and spherical space, but these three tessellations deviate in curvature the least from flat Euclidean space, which makes them the strongest candidates for a comparison with self-assembled 3D structures. Because cubes already tessellate Euclidean space, and icosahedral tessellations exist only in hyperbolic space, we do not simulate these two shapes [48]. All self-assembly simulations were carried out at constant pressure and constant N. Figure 1(d) shows equations of state for all three shapes. The data indicate a first-order transition from the disordered fluid phase into a crystalline phase for the tetrahedron and dodecahedron systems. Although a first-order transition is not evident in the octahedron data, we suspect this is simply due to the necessarily small system size [50,51].

The crystal structures that self-assemble above the transition pressure (or corresponding density) are quantified by two different types of radial distribution functions (RDF); see Figs. 1(b) and 1(c). The RDF $g_c(r)$ quantifies spatial correlations between particle centroids, and develops peaks that coincide with the characteristic geodesic distances between cells of the ideal 4-polytopes. Similarly, the RDF $g_v(r)$ calculated from the polyhedron vertices develops peaks that fit the dual lattices of the 600-cell

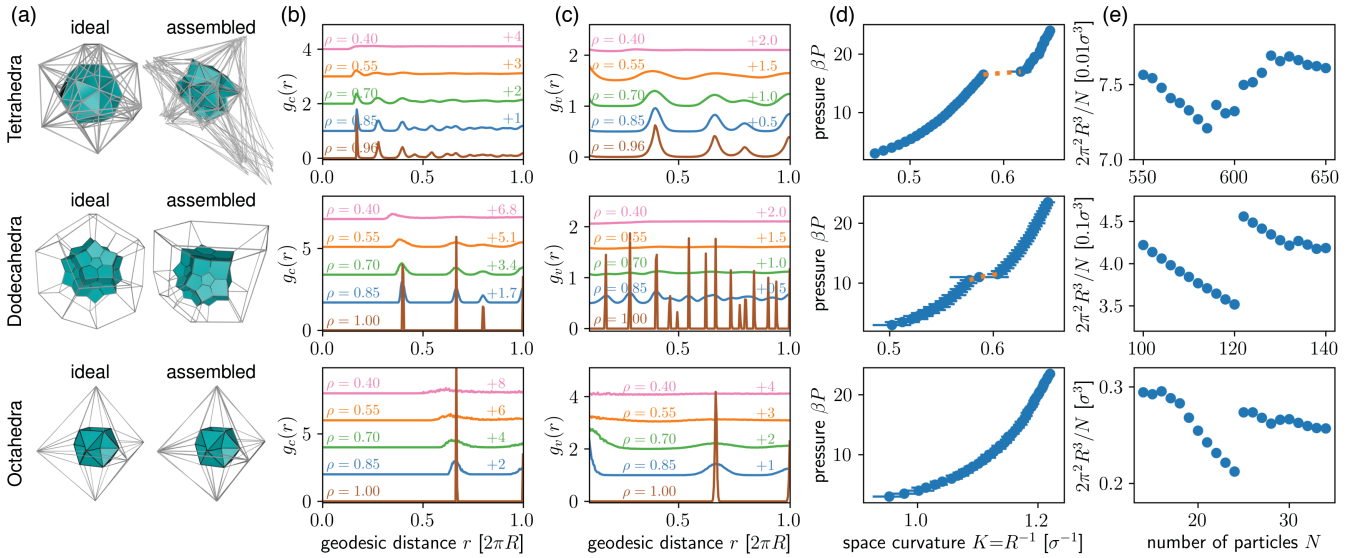

FIG. 1. Self-assembly of 600 hard tetrahedra into the 600-cell (top row), 120 hard dodecahedra into the 120-cell (center row), and 24 hard octahedra into the 24-cell (bottom row) on the 3-sphere. (a) Stereographic projections of the ideal 4-polytopes and the densest obtained assembled configuration via MC simulations. Particles that are highly deformed by the stereographic projection are outlined by their edges for better visualization. Normalized radial distribution functions at different densities ρ in regard to the (b) center positions and (c) vertex positions of the particles. (d) Space curvature vs pressure calculations during the phase transition. (e) Highest densities obtained from self-assembly simulations at different number of particles N.

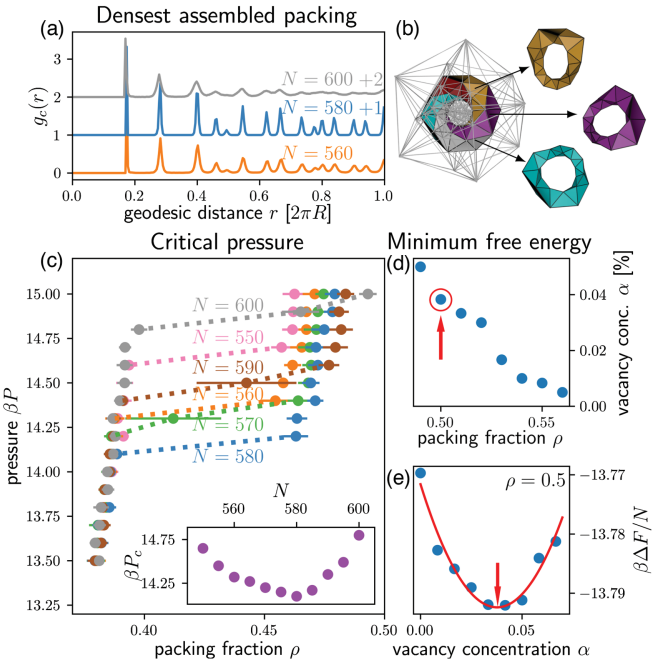

FIG. 2. (a) Normalized radial distribution functions $g_c(r)$ at the highest obtained density for 560, 580, and 600 hard tetrahedra on the 3-sphere. (b) Stereographic projections of tetrahelix loops extracted from an ideal 600-cell. (c) Pressure calculations during the phase transition for different numbers of hard tetrahedra on the 3-sphere. The inset plot shows the critical densities at the phase transition. (d) Vacancy concentration with the lowest per-particle free energy at different packing fractions. We used the Frenkel-Ladd method (see SM [41]) to calculate the free energy difference ΔF relative to an Einstein crystal. (e) Free energy difference at different vacancy concentrations for $\rho = 0.5$. The red arrows indicate the relation between (d) and (e).

(dual: 120-cell), 120-cell (dual: 600-cell) and 24-cell (self-dual). Moreover, we observe that during the formation of the 120-cell, the dodecahedron particles first achieve translational order before they align their orientations, indicating a transition from the isotropic phase into a plastic 120-cell and then into a 120-cell crystal. The existence of the plastic phase is consistent with earlier numerical studies of hard spheres that form 120-cell configurations [52].

By further increasing the density in the 24 octahedra and 120 dodecahedra system, the peaks of $g_c(r)$ and $g_v(r)$ narrow into delta functions, indicating space-filling ideal packings. Also, the stereographic projections of the self-assembled structures reveal the formation of the tessellations [see Fig. 1(a) herein and Movies 1–3 in SM [41]]. We were unable to compress the 600 tetrahedra into the perfect tiling of the 3-sphere; instead, we observe a 600-cell with void defects and interstitials at a maximum density $\rho = 0.96$.

Defect stabilized 600-cell.—To determine why the perfect 600-cell tessellation of tetrahedra does not assemble at high densities we performed additional simulations with slightly lower and higher numbers of particles [see Fig. 1(e)]. Whereas the octahedron and dodecahedron 3-sphere systems are the most densely packed for the ideal number of particles that correspond to their 4-polytopes, the tetrahedron systems create the lowest local density for $N = 585$ when defects are present (see Movie 4 in SM [41]). Also, the critical pressures at the phase transition and free energy calculations in Fig. 2 indicate that the 600-cell spherical lattice is stabilized by impurities at the transition with $N = 585$. This stabilization of the crystalline phase via vacancies is similar to the equilibrium sc phase of hard cubes [17], where cubes form linear arrays that can slide along each other adding another entropic contribution and leading to the stabilization of the sc crystal via the inclusion of void defects. Analogously, the 600-cell can be separated into 20 linear arrays known as tetrahelix loops, indicating a similar sliding mechanism [53] [see Fig. 2(b)]. While our calculations in Fig. 2(d) show that a 600-cell with a 5% void defect concentration minimizes free energy at the phase transition ($\rho \approx 0.5$), they also suggest that the hard tetrahedron system should eventually eliminate the vacancies at higher densities, like hard cubes do in Euclidean space. Consequently, our system of hard tetrahedra confined to the 3-sphere does not reach proper equilibrium beyond $\rho > 0.56$ but is configurationally trapped instead. Our compression scheme even when allowing temporary overlaps [54], therefore, is unable to eliminate defects integrated into the crystal structure after its initial assembly, resulting in a defected 600-cell.

Bending into flat space.—To study how assemblies in Euclidean space resolve geometrical incompatibilities so that particles can arrange into entropically favored configurations, we frustrated the 24-, 120-, and 600-cell structures from curved space into Euclidean space. Specifically, we increased the number of particles on the 3-sphere, which simultaneously decreases the space curvature $K = (2\pi^2\rho_N/N)^{2/3}$ at a constant number density ρ_N. As the flattening systems gradually incorporate more particles, the larger the 3-sphere radius deviates from the ideal curvature that allows for tessellation. Hence, we repeated our numerical calculations with $N_{\mathrm{oct}} \in [26, 480]$, $N_{\mathrm{dod}} \in [125, 1000]$, and $N_{\mathrm{tet}} \in [620, 1000]$ by running separate simulations for each N. We quantified the assemblies locally by calculating a set of Minkowski order parameters (MOPs) q_4, q_5, q_6, q_8, q_{10}, and q_{12} [55,56] (see SM [41]). When we slightly increase the number of particles from the ideal number that can tessellate the 3-sphere perfectly, local environments are introduced that deviate from their ideal 4-polytope arrangements in all three systems. Consequently, the region of typical particle environments expands in the six-dimensional MOP space, while most particles keep 4-polytope-like environments (see Fig. 3 herein and Figs. SI1–SI3 in SM).

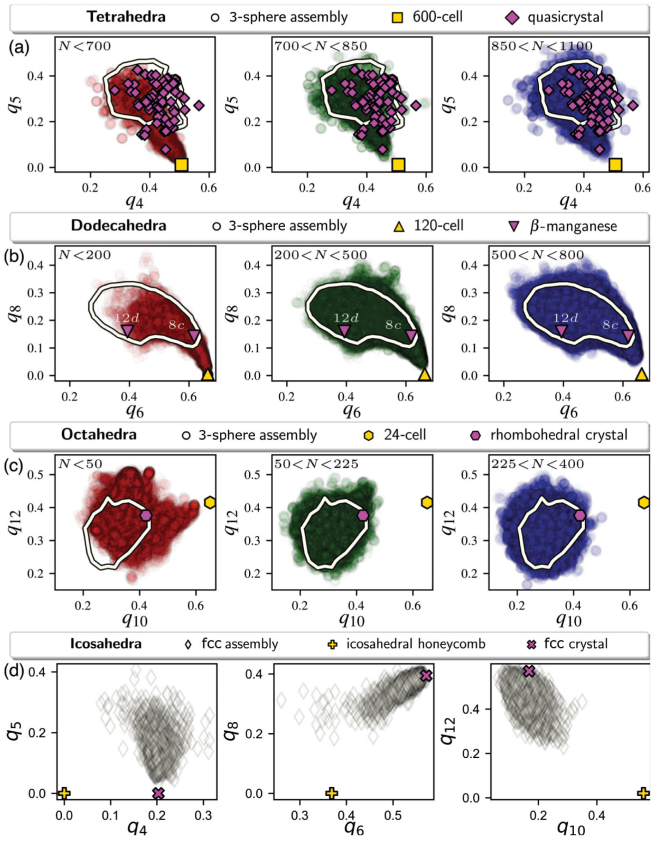

FIG. 3. Minkowski order parameter of hard (a) tetrahedron (q_4/q_5), (b) dodecahedron (q_6/q_8), and (c) octahedron (q_{10}/q_{12}) assemblies on the 3-sphere at $\rho = 0.65$ with a small (left, red), medium (center, green), and large (right, blue) degree of flattening into Euclidean space. The curvature $K \propto N^{-2/3}$ is regulated by the number of particles N. The remaining set of MOPs are shown in Figs. SI1–SI3 in SM [41]. Each circle represents a particle environment obtained from the simulation. The white outline indicates the region within which 80% of the typical local particle environments of the self-assembled structures in Euclidean space lie (β-manganese for dodecahedra with Wyckoff sites $8c$ and $12d$, quasicrystal for tetrahedra, and rhombohedral crystals for octahedra). For the tetrahedra we use the $(3, 4, 3^2, 4)$ quasicrystal approximant of the dodecagonal quasicrystal as a reference [19]. (d) Comparison between the MOP of hard icosahedra in their densest packings (flat space: fcc; hyperbolic space: icosahedral honeycomb) and a self-assembled fcc structure in Euclidean space.

For the dodecahedron and tetrahedron systems, this region of local environments characterized by MOPs remains consistent even for a large number of added particles (i.e., considerable flattening) and can also be identified as the typical environments of their representative ideal and thermalized self-assembled structures in Euclidean space: the β-manganese structure for dodecahedra and the quasicrystal for tetrahedra. Moreover, the development of the local environments with decreasing K indicates why these systems feature multiple local particle arrangements in Euclidean space. The unit cell

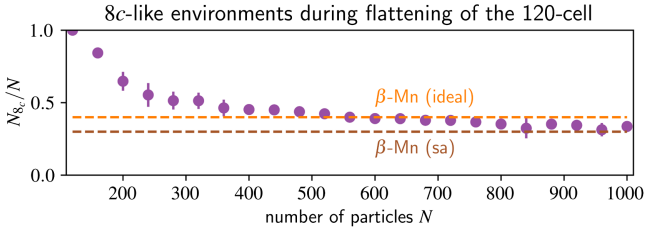

FIG. 4. Ratio of hard dodecahedra in assemblies on the 3-sphere with local environments closer to the $8c$ rather than the $12d$ Wyckoff site of the ideal β-manganese structure in MOP space. The same data are used as in Fig. 3(b). The orange dotted line refers to the ideal ratio of $8c$ particles in the β-manganese crystal $(N_{8c}/N)_{\text{ideal}} = 0.4$. The red dashed line refers to the obtained ratio when we apply the same calculations to a self-assembled β-manganese structure of hard dodecahedra in Euclidean space $(N_{8c}/N)_{\text{sa}} = 0.31 \pm 0.02$.

of the β-manganese crystal lattice, for example, contains 20 atoms with two unique Wyckoff sites $8c$ and $12d$ and, hence, two different local environments. The Wyckoff sites are located in two different regions within the MOP space. Remarkably, $8c$ is in close vicinity to the ideal 120-cell environment such that some hard dodecahedra in simulations with $N = 120$ adopt $8c$-like environments due to fluctuations. By assigning each environment during the flattening process to one of the Wyckoff sites depending on their distance in MOP space (see Fig. 4), we identify $8c$, with its 12 local neighbors, as inherited from the 3-sphere tessellation whereas $12d$ (14 neighbors) is a disclination integrated into the 120-cell structure. This becomes apparent by considering that the coordination shell of $12d$ can be generated by adding a dislocation line to the coordination shell of $8c$ [25,31]. In assemblies with a small number of added dodecahedra $N \in [120, 200]$ the particles arrange mostly in an $8c$-like local environment with only a few particles accumulating around the $12d$ environment. By flattening space further, the number of $12d$-like environments increases, which is in accordance with the addition of more disclination lines. The ratio between $8c$- and $12d$-like particles converges toward a value between the ideal ratio of sites in a β-manganese crystal $(N_{8c}/N) = (8/20) = 0.4$ and a ratio obtained from a self-assembled β-manganese crystal $(N_{8c}/N) = 0.31 \pm 0.02$.

Similarly, the multiple environments in the quasicrystal of hard tetrahedra can be interpreted as defects. Even by comparing the MOPs between a quasicrystal and the self-assembled 600-cell structure with void defects we detect that the local environments match (see Fig. SI4 [41]). By flattening space, more and more particles obtain the quasicrystalline environments. We, therefore, argue that the quasicrystal is a result of the entropic gain to integrate different defects into the 600-cell that allows for the development of a variety of different local environments that we interpret as vacancies and interstitials in the 600-cell.

However, hard octahedron systems with many added particles $N_{\mathrm{oct}} > 50$ paint a different picture. Here, the octahedron assembly must overcome a larger curvature difference to flatten the 24-cell ($\Delta K_{24} \approx 1.571\sigma^{-2}$) compared to the 120-cell ($\Delta K_{120} \approx 0.776\sigma^{-2}$) or 600-cell ($\Delta K_{600} \approx 0.764\sigma^{-2}$). Therefore, the strategy of entropy compartmentalization [57,58] by adding defects to the 24-cell eventually becomes less efficient than maximizing entropy by forming crystals with only one type of local environment reminiscent of the rhombohedral crystal. The switch of entropy minimization mechanisms is apparent in Fig. 3(c) herein and Fig. SI3 in SM [41], where the octahedra do not adopt local environments close to those in the 24-cell for large N. This phenomenon draws similarities to frustration escape in geometrically frustrated assemblies (GFAs) of deformable particles with open boundaries [59–62]. Despite not being dominated by entropy but instead energetic contributions such as particle deformation, binding between building blocks, and boundary energy terms, GFAs also feature an incompatibility between the locally preferred order and global constraints. Similar to the space curvature in our hard particle assemblies, the particle shape rigidity in GFAs dictates if it is energetically more favorable for the system to accumulate stresses without losing locally preferred order (rigid self-limiting regime) or to escape the frustration by deforming the particles (soft bulk regime). Hence, the self-assembled structure of hard octahedra is not based on a 3-sphere tessellation. Instead, the assembly is more related to the densest packing in Euclidean space, which indicates how to accommodate global and local geometric frustration uniformly.

Although we cannot perform a similar computational study with icosahedra as its tessellation, the icosahedral honeycomb (ih), only exists in negatively curved hyperbolic three-space, we observe in Fig. 3(d) that the typical local environments of the self-assembled fcc crystal of icosahedra in Euclidean space show the same characteristics as the octahedron system. Within the MOP space the icosahedra environments sit in a region close to the ideal fcc but clearly detached from the ideal ih environment. This and the existence of only one local environment in the ideal fcc crystal suggest that the occurrence of the fcc crystal in hard icosahedron systems is also caused by the large difference in curvature between the ih crystal and Euclidean space. As in the octahedron system, the geometric frustration is distributed uniformly in Euclidean space rather than concentrated by adding defects and introducing additional local environments. Therefore, we surmise that the fcc phase is not related to the ih tessellation in hyperbolic space, but rather to the densest packing in Euclidean space.

Conclusion.—In this Letter, we rationalize the assembly of complex colloidal crystal structures of hard polyhedra based on tessellations in curved space. By performing MC simulations of hard tetrahedra, octahedra, and dodecahedra on positively curved 3-spheres, we showed that the particles thermodynamically self-assemble their 4-polytope tessellations. Hence, the particles adopt their locally optimal configurations if no geometrical restrictions are present, such as those that occur when they attempt to crystallize in Euclidean space. Moreover, we observed by flattening space that equilibrium colloidal crystal structures in Euclidean space can be separated into two categories. The first category includes self-assembled structures with multiple local environments in flat space that can be understood as remnants of perfect tessellations in curved space indicating the predictive power of curved tessellations and curved crystal for Euclidean assemblies. As an example, we traced back the dodecagonal quasicrystal phase of hard tetrahedra to the 600-cell and its low entropic cost to implement void defects into the crystal. Likewise, the β-manganese configuration of hard dodecahedra stems from the 120-cell, with the two Wyckoff sites of the crystal identified as a local environment native to the 120-cell and a defect, respectively. The second category includes self-assembled Euclidean crystals that do not stem from tessellations in curved space, such as the rhombohedral crystal of hard octahedra or the fcc crystal of hard icosahedra. Their corresponding tessellations require spaces with considerably larger curvature resulting in a frustration escape [59–62]. Consequently, these assemblies adopt a geometric compromise in Euclidean space where entropy maximization is achieved uniformly through a characteristic single local environment instead of introducing defects.

Although we focused on the hard-core limit exclusively in this study, our findings are also relevant for systems with enthalpic contributions considering the mathematical description of Frank-Kapser phases as disclinated 600-cells [27,28]. Furthermore, it is well established that altering the features of particle interactions, such as their softness, changes the stability of competing crystalline structures [63–66] and affects the glass-forming ability of packings which corresponds to their capability to resolve frustration [67,68]. Therefore, introducing a soft repulsion between the polyhedra, allowing shape deformations with an associated energy penalty, or tuning interparticle stresses [61,62] grants the system additional degrees of freedom to resolve geometric frustration during the space-flattening process. These modifications can theoretically broaden and control the curvature window, where assemblies based on non-Euclidean crystals minimize free energy and, for instance, help us identify the Euclidean remnant of the 24-cell. Hence, our results not only provide a fundamental theoretical explanation behind the plethora of existing colloidal crystal structures but also open an avenue to discover and guide the prediction of new self-assembly structures that are based on curved crystals and tessellations.

The authors thank Nicholas Kotov, Nan Cheng, and Francesco Serafin for helpful discussions. X M. and K. S. were supported in part by the Office of Naval Research (MURI N00014-20-1-2479), and by the National Science Foundation (NSF PHY-1748958); P. W. A. S. and S. C. G. were supported by a grant from the Simons Foundation (No. 256297, S. C. G.). This work used the Extreme Science and Engineering Discovery Environment (XSEDE), which is supported by National Science Foundation Grant No. ACI-1548562; XSEDE Grant No. DMR 140129. Computational resources and services were also supported by Advanced Research Computing at the University of Michigan, Ann Arbor.

*sglotzer@umich.edu

[1] J. A. Champion, Y. K. Katare, and S. Mitragotri, Particle shape: A new design parameter for micro- and nanoscale drug delivery carriers, J. Control. Release **121**, 3 (2007).
[2] J. Lee, K. H. Ku, J. Kim, Y. J. Lee, S. G. Jang, and B. J. Kim, Light-responsive, shape-switchable block copolymer particles, J. Am. Chem. Soc. **141**, 15348 (2019).
[3] J. Wu, C. Ruan, Y. Ma, Y. Wang, and Y. Luo, Vital role of hydroxyapatite particle shape in regulating the porosity and mechanical properties of the sintered scaffolds, J. Mater. Sci. Technol. **34**, 503 (2018).
[4] M. R. Jones, R. J. Macfarlane, B. Lee, J. Zhang, K. L. Young, A. J. Senesi, and C. A. Mirkin, DNA-nanoparticle superlattices formed from anisotropic building blocks, Nat. Mater. **9**, 913 (2010).
[5] Y. Zhang, F. Lu, K. G. Yager, D. van der Lelie, and O. Gang, A general strategy for the DNA-mediated self-assembly of functional nanoparticles into heterogeneous systems, Nat. Nanotechnol. **8**, 865 (2013).
[6] Z. J. Urbach, S. S. Park, S. L. Weigand, J. E. Rix, B. Lee, and C. A. Mirkin, Probing the consequences of cubic particle shape and applied field on colloidal crystal engineering with DNA, Angew. Chem. **133**, 4111 (2021).
[7] I. Zuriguel and T. Mullin, The role of particle shape on the stress distribution in a sandpile, Proc. R. Soc. A **464**, 99 (2008).
[8] S. Wegner, R. Stannarius, A. Boese, G. Rose, B. Szabo, E. Somfai, and T. Börzsönyi, Effects of grain shape on packing and dilatancy of sheared granular materials, Soft Matter **10**, 5157 (2014).
[9] K. A. Murphy, K. A. Dahmen, and H. M. Jaeger, Transforming mesoscale granular plasticity through particle shape, Phys. Rev. X **9**, 011014 (2019).
[10] P. F. Damasceno, M. Engel, and S. C. Glotzer, Predictive self-assembly of polyhedra into complex structures, Science **337**, 453 (2012).
[11] G. van Anders, D. Klotsa, A. S. Karas, P. M. Dodd, and S. C. Glotzer, Digital alchemy for materials design: Colloids and beyond, ACS Nano **9**, 9542 (2015).
[12] Y. Geng, G. van Anders, P. M. Dodd, J. Dshemuchadse, and S. C. Glotzer, Engineering entropy for the inverse design of colloidal crystals from hard shapes, Sci. Adv. **5**, eaaw0514 (2019).
[13] M. Z. Miskin, G. Khaira, J. J. de Pablo, and H. M. Jaeger, Turning statistical physics models into materials design engines, Proc. Natl. Acad. Sci. U.S.A. **113**, 34 (2016).
[14] G. M. Coli, E. Boattini, L. Filion, and M. Dijkstra, Inverse design of soft materials via a deep learning–based evolutionary strategy, Sci. Adv. **8**, eabj6731 (2022).
[15] T. Vo and S. C. Glotzer, A theory of entropic bonding, Proc. Natl. Acad. Sci. U.S.A. **119**, e2116414119 (2022).
[16] B. A. Schultz, P. F. Damasceno, M. Engel, and S. C. Glotzer, Symmetry considerations for the targeted assembly of entropically stabilized colloidal crystals via voronoi particles, ACS Nano **9**, 2336 (2015).
[17] F. Smallenburg, L. Filion, M. Marechal, and M. Dijkstra, Vacancy-stabilized crystalline order in hard cubes, Proc. Natl. Acad. Sci. U.S.A. **109**, 17886 (2012).
[18] S. Torquato and Y. Jiao, Dense packings of the Platonic and Archimedean solids, Nature (London) **460**, 876 (2009).
[19] A. Haji-Akbari, M. Engel, and S. C. Glotzer, Phase diagram of hard tetrahedra, J. Chem. Phys. **135**, 194101 (2011).
[20] A. Haji-Akbari, M. Engel, and S. C. Glotzer, Degenerate quasicrystal of hard triangular bipyramids, Phys. Rev. Lett. **107**, 215702 (2011).
[21] E. R. Chen, M. Engel, and S. C. Glotzer, Dense crystalline dimer packings of regular tetrahedra, Discrete Comput. Geom. **44**, 253 (2010).
[22] E. R. Chen, D. Klotsa, M. Engel, P. F. Damasceno, and S. C. Glotzer, Complexity in surfaces of densest packings for families of polyhedra, Phys. Rev. X **4**, 011024 (2014).
[23] D. Klotsa, E. R. Chen, M. Engel, and S. C. Glotzer, Intermediate crystalline structures of colloids in shape space, Soft Matter **14**, 8692 (2018).
[24] G. van Anders, D. Klotsa, N. K. Ahmed, M. Engel, and S. C. Glotzer, Understanding shape entropy through local dense packing, Proc. Natl. Acad. Sci. U.S.A. **111**, E4812 (2014).
[25] J. F. Sadoc, Periodic networks of disclination lines: Application to metal structures, J. Phys. Lett. **44**, 707 (1983).
[26] J. F. Sadoc and R. Mosseri, Disclination density in atomic structures described in curved spaces, J. Phys. (Les Ulis, Fr.) **45**, 1025 (1984).
[27] M. Kléman, Curved crystals, defects and disorder, Adv. Phys. **38**, 605 (1989).
[28] A. Travesset, Nanoparticle superlattices as quasi-Frank-Kasper phases, Phys. Rev. Lett. **119**, 115701 (2017).
[29] M. Kleman and J. F. Sadoc, A tentative description of the crystallography of amorphous solids, J. Phys. Lett. **40**, 569 (1979).
[30] J. F. Sadoc, Use of regular polytopes for the mathematical description of the order in amorphous structures, J. Non-Cryst. Solids **44**, 1 (1981).
[31] D. R. Nelson, Order, frustration, and defects in liquids and glasses, Phys. Rev. B **28**, 5515 (1983).
[32] D. R. Nelson, Liquids and glasses in spaces of incommensurate curvature, Phys. Rev. Lett. **50**, 982 (1983).
[33] R. Mosseri and J. F. Sadoc, Hierarchical structure of defects in non-crystalline sphere packings, J. Phys. Lett. **45**, 827 (1984).
[34] G. Venkataraman and D. Sahoo, Curved space and amorphous structures Part I. Geometric models, Contemp. Phys. **26**, 579 (1985).

[35] J. P. Straley, Crystallization in curved three-dimensional space, Phys. Rev. B **30**, 6592 (1984).
[36] F. Serafin, J. Lu, N. Kotov, K. Sun, and X. Mao, Frustrated self-assembly of non-Euclidean crystals of nanoparticles, Nat. Commun. **12**, 1 (2021).
[37] J. P. Sethna, D. C. Wright, and N. D. Mermin, Relieving cholesteric frustration: The blue phase in a curved space, Phys. Rev. Lett. **51**, 467 (1983).
[38] J. P. Sethna, Frustration, curvature, and defect lines in metallic glasses and the cholesteric blue phase, Phys. Rev. B **31**, 6278 (1985).
[39] B. G. Chen, P. J. Ackerman, G. P. Alexander, R. D. Kamien, and I. I. Smalyukh, Generating the Hopf fibration experimentally in nematic liquid crystals, Phys. Rev. Lett. **110**, 237801 (2013).
[40] J.-F. Sadoc, R. Mosseri, and J. V. Selinger, Liquid crystal director fields in three-dimensional non-Euclidean geometries, New J. Phys. **22**, 093036 (2020).
[41] See Supplemental Material at http://link.aps.org/supplemental/10.1103/PhysRevLett.131.258201 for numerical methods, which include Refs. [42–46].
[42] J. A. Anderson, J. Glaser, and S. C. Glotzer, HOOMD-blue: A Python package for high-performance molecular dynamics and hard particle Monte Carlo simulations, Comput. Mater. Sci. **173**, 109363 (2020).
[43] D. W. Sinkovits, S. A. Barr, and E. Luijten, Rejection-free Monte Carlo scheme for anisotropic particles, J. Chem. Phys. **136**, 144111 (2012).
[44] G. Snethen, Xenocollide: Complex collision made simple, *Game Programming Gems 7* (Course Technology, Boston, 2008), pp. 165–178.
[45] D. Frenkel and A. J. C. Ladd, New Monte Carlo method to compute the free energy of arbitrary solids. Application to the fcc and hcp phases of hard spheres, J. Chem. Phys. **81**, 3188 (1984).
[46] D. Frenkel and B. Smit, *Understanding Molecular Simulation: From Algorithms to Applications* (Elsevier, New York, 2001), Vol. 1.
[47] G. Turci, A. Tarjus, and C. P. Royall, From glass formation to icosahedral ordering by curving three-dimensional space, Phys. Rev. Lett. **118**, 215501 (2017).
[48] A first attempt to perform simulations in hyperbolic space investigated only hard spheres [49].
[49] C. D. Modes and R. D. Kamien, Hard disks on the hyperbolic plane, Phys. Rev. Lett. **99**, 235701 (2007).
[50] K. Binder and D. P. Landau, Finite-size scaling at first-order phase transitions, Phys. Rev. B **30**, 1477 (1984).
[51] V. Privman and M. E. Fisher, Finite-size effects at first-order transitions, *Current Physics–Sources and Comments* (Elsevier, New York, 1988), Vol. 2, pp. 149–181.
[52] R. Jullien, J. F. Sadoc, and R. Mosseri, Packing at random in curved space and frustration: A numerical study, J. Phys. I **7**, 1677 (1997).
[53] J. F. Sadoc, Helices and helix packings derived from the {3, 3, 5} polytope, Eur. Phys. J. E **5**, 575 (2001).
[54] A. Haji-Akbari, M. Engel, A. S. Keys, X. Zheng, R. G. Petschek, P. Palffy-Muhoray, and S. C. Glotzer, Disordered, quasicrystalline and crystalline phases of densely packed tetrahedra, Nature (London) **462**, 773 (2009).
[55] P. J. Steinhardt, D. R. Nelson, and M. Ronchetti, Bond-orientational order in liquids and glasses, Phys. Rev. B **28**, 784 (1983).
[56] W. Mickel, S. C. Kapfer, G. E. Schröder-Turk, and K. Mecke, Shortcomings of the bond orientational order parameters for the analysis of disordered particulate matter, J. Chem. Phys. **138**, 044501 (2013).
[57] T. C. Moore, J. A. Anderson, and S. C. Glotzer, Shape-driven entropic self-assembly of an open, reconfigurable, binary host–guest colloidal crystal, Soft Matter **17**, 2840 (2021).
[58] S. Lee, T. Vo, and S. C. Glotzer, Entropy compartmentalization stabilizes open host–guest colloidal clathrates, Nat. Chem. **15**, 1 (2023).
[59] D. M. Hall and G. M. Grason, How geometric frustration shapes twisted fibres, inside and out: Competing morphologies of chiral filament assembly, Interface Focus **7**, 20160140 (2017).
[60] M. F. Hagan and G. M. Grason, Equilibrium mechanisms of self-limiting assembly, Rev. Mod. Phys. **93**, 025008 (2021).
[61] I. R. Spivack, D. M. Hall, and G. M. Grason, Stress accumulation versus shape flattening in frustrated, warped-jigsaw particle assemblies, New J. Phys. **24**, 063023 (2022).
[62] D. M. Hall, M. J. Stevens, and G. M. Grason, Building blocks of non-Euclidean ribbons: Size-controlled self-assembly via discrete frustrated particles, Soft Matter **19**, 858 (2023).
[63] R. A. LaCour, C. S. Adorf, J. Dshemuchadse, and S. C. Glotzer, Influence of softness on the stability of binary colloidal crystals, ACS Nano **13**, 13829 (2019).
[64] T. Dasgupta, G. M. Coli, and M. Dijkstra, Tuning the glass transition: Enhanced crystallization of the laves phases in nearly hard spheres, ACS Nano **14**, 3957 (2020).
[65] P. W. A. Schönhöfer, M. Marechal, D. J. Cleaver, and G. E. Schröder-Turk, Self-assembly and entropic effects in pear-shaped colloid systems. I. Shape sensitivity of bilayer phases in colloidal pear-shaped particle systems, J. Chem. Phys. **153**, 034903 (2020).
[66] Z. W. Li, Y. W. Sun, Y. H. Wang, Y. L. Zhu, Z. Y. Lu, and Z. Y. Sun, Softness-enhanced self-assembly of pyrochlore- and perovskite-like colloidal photonic crystals from triblock Janus particles, J. Phys. Chem. Lett. **12**, 7159 (2021).
[67] K. Zhang, M. Fan, Y. Liu, J. Schroers, M. D. Shattuck, and C. S. O'Hern, Beyond packing of hard spheres: The effects of core softness, non-additivity, intermediate-range repulsion, and many-body interactions on the glass-forming ability of bulk metallic glasses, J. Chem. Phys. **143**, 184502 (2015).
[68] A. Ninarello, L. Berthier, and D. Coslovich, Models and algorithms for the next generation of glass transition studies, Phys. Rev. X **7**, 021039 (2017).